

### **OPEN ACCESS**

EDITED BY

Muhammad Imran Rashid, University of Engineering and Technology, Lahore, Pakistan

REVIEWED BY
Yujun Xu,
Anhui University of Science and
Technology, China
Qingxiang Wang,
China University of Mining and

Technology, China
\*CORRESPONDENCE

Xiaoru Wu,

■ duangang@cumt.edu.cn

RECEIVED 22 September 2025 REVISED 19 October 2025 ACCEPTED 27 October 2025 PUBLISHED 17 November 2025

### CITATION

Jin F, Wu X, Liu Z, Pan H and Shong T (2025) Influence of slurry mass concentration on the mineralization capacity and mechanical properties of coal-based solid wastes. *Front. Mater.* 12:1710858. doi: 10.3389/fmats.2025.1710858

### COPYRIGHT

© 2025 Jin, Wu, Liu, Pan and Shong. This is an open-access article distributed under the terms of the Creative Commons Attribution License (CC BY). The use, distribution or reproduction in other forums is permitted, provided the original author(s) and the copyright owner(s) are credited and that the original publication in this journal is cited, in accordance with accepted academic practice. No use, distribution or reproduction is permitted which does not comply with these terms.

# Influence of slurry mass concentration on the mineralization capacity and mechanical properties of coal-based solid wastes

Feng Jin<sup>1</sup>, Xiaoru Wu<sup>2</sup>\*, Zhicheng Liu<sup>3</sup>, Hao Pan<sup>2</sup> and Tianqi Shong<sup>2</sup>

<sup>1</sup>China National Coal Group Corporation, Bei'jing, China, <sup>2</sup>China Coal Energy Research Institute Co., Ltd, Xi'an, China, <sup>3</sup>College of Energy and Mining Engineering, Xi'an University of Science and Technology, Xi'an, China

The CO<sub>2</sub>-mineralized coal-based solid waste backfilling is an effective method for solid waste treatment and carbon sequestration. Both the carbon sequestration capacity, rheological properties and unconfined compressive strength (UCS) of the CO<sub>2</sub>-mineralized coal-based solid waste backfill material (CO<sub>2</sub>-CBM) are key evaluation indicators for its application and promotion. To optimize the engineering performance of  $\mathrm{CO}_2\mathrm{-CBM}$ , the influence mechanism of slurry mass concentration (65%-73%) on its carbon sequestration capacity, rheological properties and UCS was systematically studied. Study results show that the carbon sequestration rate of CO<sub>2</sub>-CBM decreases with the increase of slurry mass concentration. Over a period of time, the carbon sequestration amount also decreases with the increase of slurry mass concentration, reaching 82.4 g/kg at the mass concentration of 65%. Both the extension of the standing time and the increase in mass concentration significantly rise the flow resistance of CO<sub>2</sub>-CBM. When the mass concentration is 73% and the standing time is 30 min, the yield stress and plastic viscosity of CO<sub>2</sub>-CBM reach 281.84 Pa and 0.95 Pa·s. The results of microscopic analysis show that due to the higher concentration of C-S-H in the slurry, CO2-CBM exhibits a denser structure and lower porosity. Consequently, as the slurry mass concentration increases, the UCS of the CO<sub>2</sub>-CBM is significantly improved, and the UCS reaches 3.30 MPa at the slurry mass concentration of 73% after a standing time of 28 days. This research provides a basis for optimizing key parameters for the co-processing of solid waste and CO<sub>2</sub> in coal mine goaf.

KEYWORDS

coal-based solid waste, mass concentration, carbon sequestration performance, rheological properties, uniaxial compressive strength

### 1 Introduction

In recent years, global carbon emissions have been increasing year by year. In 2024, the carbon emissions reached as high as 37.8 Gt (IEA, 2025), leading to a series of climate problems. Therefore, the reduction of carbon emissions has become an urgent priority. A large number of goafs generated during coal mining

provide potential space for the mineralization and storage of  $\mathrm{CO}_2$  (Lang et al., 2022; Shuangming et al., 2023). Heping et al. (2018) predicted that by 2030, the underground space of goafs in Chinese coal mines alone would reach 23.4 billion cubic meters. In addition, coal mine backfilling mining technology has been gradually promoted and applied. Therefore, using  $\mathrm{CO}_2$ -mineralized coal-based solid wastes to prepare backfilling materials offers an efficient approach for achieving both  $\mathrm{CO}_2$  sequestration and solid waste management.

Cemented backfill mining is one of the core techniques of backfill mining (Minggao et al., 2018), which can be used to effectively control the movement of overlying strata and minimize surface subsidence in the goaf. In this technique, bulk coal-based solid wastes such as coal gangue and fly ash are used as raw materials, enhancing the resource utilization rate of coal-based solid wastes. This approach realizes the environmental protection concept of "Originating from coal-based solid waste and returning to its management" (Shuangming et al., 2024), and improves the economic, environmental and social benefits of coal production (Tingye et al., 2025). It is crucial to study the conveying performance and compressive resistance performance of the prepared cemented backfilling material (CBM) to ensure it can be smoothly pumped into the goaf and solidified with a certain load-bearing capacity. At present, researchers have conducted relatively in-depth research on the mechanical properties of traditional coal-based solid waste CBMs. Zhang et al. (2022) tested the influence of mass concentration and ash-gangue ratio on the UCS of coal-based solid waste cemented materials, and initially prepared a multi-source coal-based solid waste CBM. Wei et al. (2022) constructed a multiple nonlinear regression model for the strength of backfill bodies at different curing ages, revealing the influence mechanism of each solid waste dosage and its interaction on the strength of the backfill body. Experiments on the influence of factors such as chlorides, moisture content (Wang et al., 2023), nanocomposite fiber, and ash content on the mechanical properties of coal-based solid waste cementitious materials (Weiji et al., 2024) have also been conducted.

In recent years, following China's introduction of the Dual Carbon Goals, the idea of negative carbon filling has emerged (Zhang et al., 2025; Ren et al., 2025; Heping et al., 2024). Researchers have started to explore the carbon capture capabilities and mechanical characteristics of backfilling materials that utilize coal-based solid waste for CO<sub>2</sub> mineralization. With its mechanical support and rapid strength development, CO2-mineralized backfill enables proactive strata control, turning coal mining into a green process for carbon sequestration, water preservation, and energy recovery. (Xu et al., 2025a; Xu et al., 2025b). Wang et al. (2025) studied the carbon sequestration capacity of calcium carbide slag, red mud and fly ash using a gas with a CO<sub>2</sub> concentration of 15%, and tested that the maximum carbon sequestration capacity of the mixed material was 14.4 kg·t <sup>-1</sup>. Compared with the unmineralized backfilling material, the mechanical properties were improved by 32.2% and the fluidity was improved by 10.8%. Zhang et al. (2025) investigated the effects of reaction temperature, initial pressure, stirring rate and liquid-solid ratio on the carbon sequestration capacity of coal gangue. Xu and Ma. (2024) experimentally studied the UCS and tensile strength of the prepared materials under different curing times and fly ash ratios. Their tests revealed that the maximum yield stress of the slurry reached 88 MPa, making it suitable for practical field applications. Zhu et al. (2025) tested the carbon sequestration potential of composite activated coal gangue under different ball milling times and calcination temperatures using inductively coupled plasma-optical emission spectrometry (ICP-OES). It was found that the leaching rate of Ca<sup>2+</sup> in coal gangue after 2 h of grinding and calcination at 500° C reached 34.28%. In addition, researchers have conducted studies on the carbon sequestration capacity and mechanical properties of acid-base activated coal gangue (Huo et al., 2023; Huo et al., 2024; Gao et al., 2015), coal-based solid waste fillers with different dosages of coal-based solid waste (Guo et al., 2024) and different cement concentrations (Chen et al., 2022).

In summary, the existing research on the carbon fixation and mechanical properties of  $\rm CO_2$ -mineralized coal-based solid waste backfilling materials ( $\rm CO_2$ -CBM) mainly focuses on the types and dosages of coal-based solid waste, different mineralization reaction conditions, and the activation conditions of raw materials. Studies on slurry concentration as a variable has not yet been discussed. However, the mass concentration is the most significant influencing factor on rheological and strength properties for traditional cemented slurry (Huang et al., 2022; Zou et al., 2023). In this study,  $\rm CO_2$ -CBMs were taken as the research object, and experiments on the carbon sequestration, transportation and load-bearing performance of the  $\rm CO_2$ -CBMs with different slurry mass concentrations were conducted. This study provides a reference for the promotion and application of  $\rm CO_2$ -CBMs.

### 2 Materials and methods

### 2.1 Materials

In this experiment, coal-based solid waste, cement, CaO and water were used to prepare CO<sub>2</sub>-CBM, and the carbon sequestration capacity, transportation and compressive resistance of CO<sub>2</sub>-CBM with different mass concentrations were explored. The physical and chemical properties of the raw materials were analyzed after they were dried at 60 °C for 2 days. The dry powder laser particle size testing (Jinan Micro and Nano Particle Instrument Co., LTD., Winner3009) was used to measure the particle size distribution of high-calcium fly ash (HFA), cement and CaO, as shown in Figure 1a. XRD tests of coal gangue (CG) and HFA were conducted using an X-ray diffractometer with a test step of 0.02°, and MDI Jade software was used for phase identification (Figure 1b). The chemical compositions of CG, HFA and cement were analyzed by X-ray fluorescence spectrometer (XRF, Panalytical Axios, Netherlands). The range of analyzed elements was 4 Be-92 U, and the quantitative range of elements was ppm-100%. Table 1 shows the chemical compositions and contents of each raw material measured.

### 2.1.1 Coal-based solid waste

The coal-based solid wastes used in the experiment included CG and HFA. CG, as the aggregate of  $\rm CO_2\text{-}CBM$ , was taken from a certain mine in Inner Mongolia, China. HFA exhibits a greater capacity for carbon sequestration than traditional fly ash. In this test, the commercial HFA was used. As shown in Figure 1 and Table 1, the main mineral phases of the selected CG include minerals

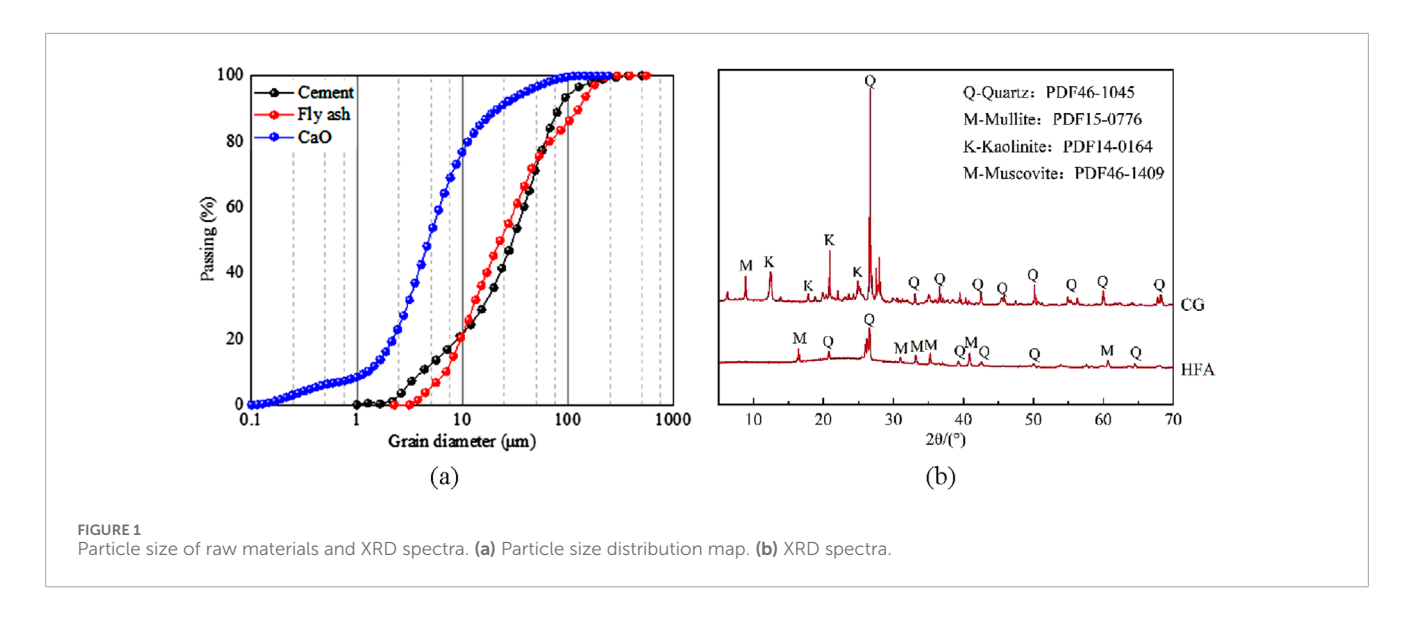


TABLE 1 Chemical composition and content of raw materials.

Type of waste	SiO <sub>2</sub> (wt%)	Al <sub>2</sub> O <sub>3</sub> (wt%)	Fe <sub>2</sub> O <sub>3</sub> (wt%)	CaO (wt%)	MgO (wt%)	Na <sub>2</sub> O (wt%)	K <sub>2</sub> O (wt%)
CG	57.434	25.219	6.515	0.481	1.713	1.692	2.874
HFA	35.11	22.66	5.53	15.08	0.94	0.874	1.32
Cement	21.34	6.74	7.68	54.15	2.61	0.50	0.92

such as quartz and kaolinite, and the main oxide components are  $SiO_2$ ,  $Al_2O_3$ , etc. The main mineral phases of HFA include quartz, mullite and other minerals. In addition to  $SiO_2$  and  $Al_2O_3$ , the main oxide components also have a CaO content of 15.08%. As shown in Figure 1, the particle size of HFA is concentrated in the range of 2.2–292.0  $\mu$ m. The initial particle size of CG was relatively large and not suitable for preparing backfill materials. After crushing and screening it, particles with a particle size of 2–5 mm were used.

### 2.1.2 Cement

The type and content of cementitious materials have a significant impact on the strength of the prepared material. In this study, P.O42.5 Portland cement produced by Zhucheng Jiuqi Building Materials Co., Ltd. Was used as the adhesive. Its particle size distribution ranged from 0.9 to 502  $\mu m$ , with a median particle size of 73  $\mu m$ . The particle size corresponding to a cumulative sieving efficiency of 90% was 85  $\mu m$ . The main components of the selected cement were CaO and SiO $_2$ .

### 2.1.3 CaO

The fundamental mechanism of mineralization involves the reaction between elements such as Ca and Mg present in the material and  $\mathrm{CO}_2$ , leading to the formation of calcium carbonate. To enhance the carbon sequestration capacity of the material, CaO was added as an additional material to the slurry. The particle size distribution range of the selected CaO was 0.1–126.7  $\mu m$ .

### 2.2 Sample preparation

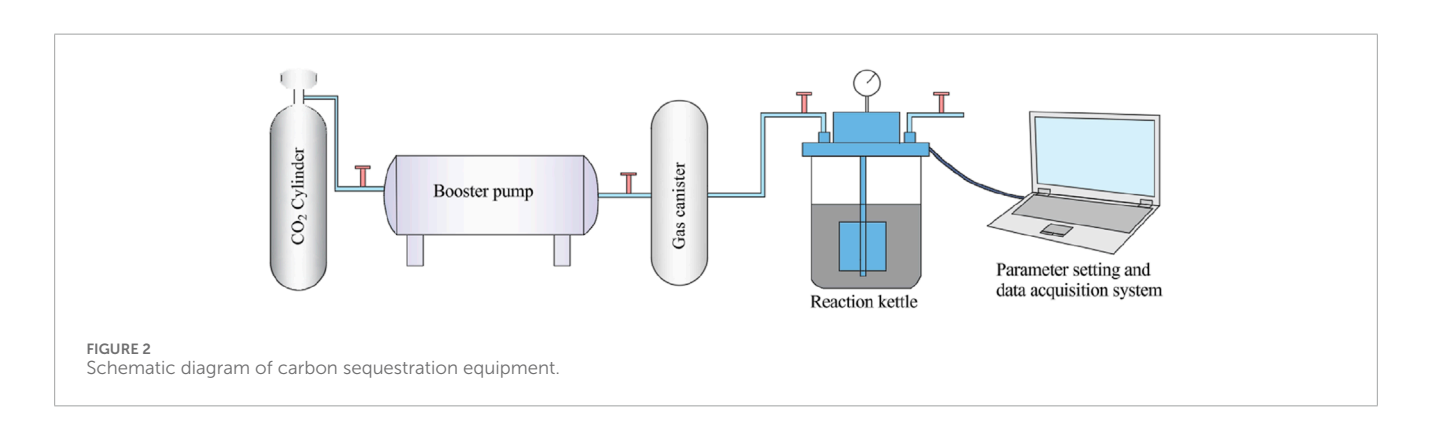
In the experimental design, the contents of CG, HFA, cement and CaO remained unchanged, with the mass concentration as the experimental variable. Based on previous research, considering that the requirements for pumpability are high and that the experiment utilized fine-grained tailings (Fall and Benzaazoua, 2005; Qi and Fourie, 2019). The slurry mass concentrations were determined to be 73%, 69%, and 65%. The specific ratios are shown in Table 2.

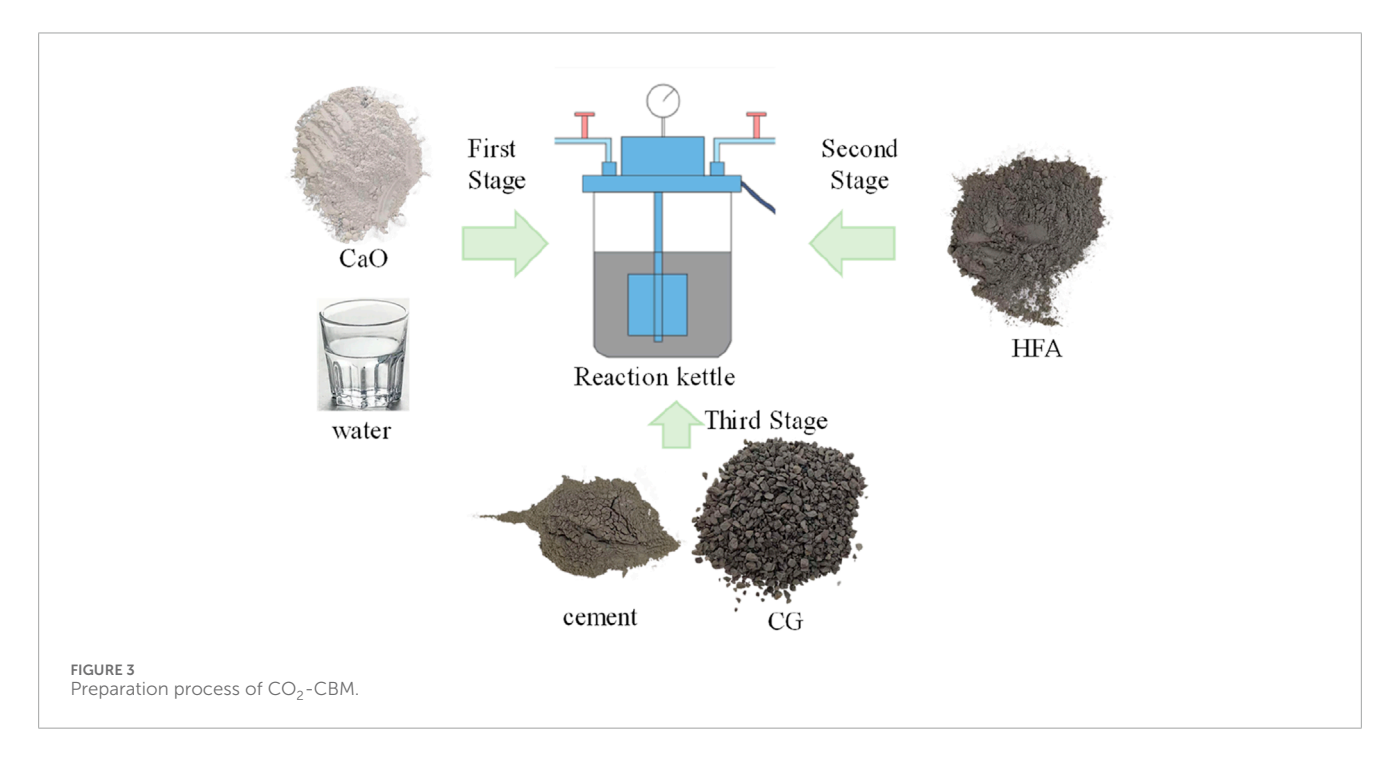
The self-made carbon fixation equipment was used to mineralize CO2-CBM, and the working principle of the equipment was demonstrated in Figure 2. The operation steps were as follows: (1) The CO<sub>2</sub> cylinder, booster pump and inlet valve of gas canister were opened, and the pressure inside the gas canister was increased to 5 MPa for standby; (2) Mineralized materials were added to the reaction kettle and the hexagonal screws were tightened on the reaction kettle. (3) In the parameter setting and data acquisition system, the CO<sub>2</sub> flow rate was set as 1.5 L/min, the stirrer speed as 900 r/min, the temperature as 25 °C, and Start Experiment was clicked to record the data; (4) After raising the pressure inside the reactor to 0.8 MPa, stirring was started and lasted for 20 min (5) After mineralization was completed, the pressure inside the reactor was reduced to normal pressure. Experiment End was clicked to disconnect all pipeline connections and the reactor was then opened.

The main carbon sequestration elements in the  $\rm CO_2\text{-}CBM$  are CaO and HFA. To explore the carbon sequestration performance

TABLE 2 Proportioning ratio for CO2-CBMs.

No.	Quicklime/%	Fly ash/%	Coal gangue/%	Cement/%	Mass concentration/%
i1	9	22	63	6	73
i2	9	22	63	6	69
i3	9	22	63	6	65



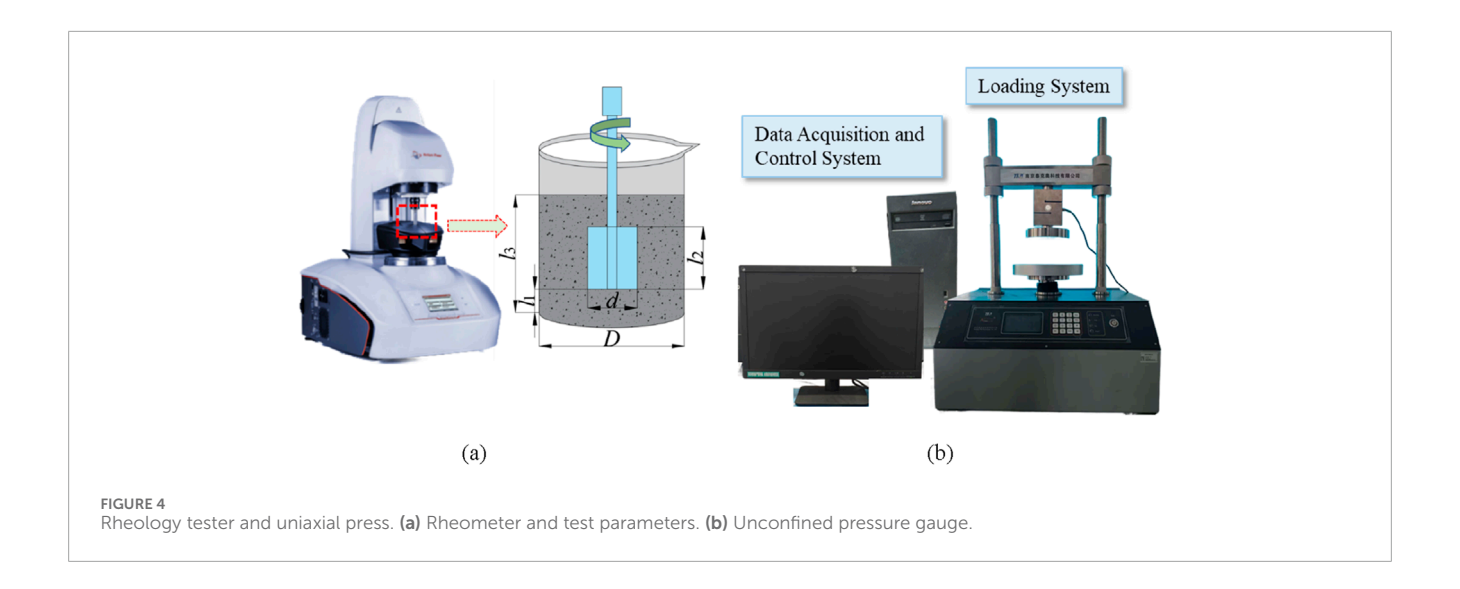


of the two materials respectively. Figure 3 shows the specific preparation process of  $\rm CO_2\text{-}CBMs$  by staged mineralization. According to the operation process of the above-mentioned equipment, the staged mineralization was accomplished in three phases. In the first stage, CaO and water were added until the reaction was completed. In the second stage, HFA was added and the mixture was reacted under identical conditions for 20 min. In the third stage, cement and CG were incorporated without introducing  $\rm CO_2$ , followed by stirring for 5 min to achieve a homogeneous mixture.

### 2.3 Test methods

### 2.3.1 Carbon sequestration capacity

Currently, three approaches are utilized to evaluate the  $\rm CO_2$  sequestration capacity of solid waste: the pressure drop method, thermogravimetric method, and the inlet-outlet flow counting method. The thermogravimetric method may cause significant errors due to the limitations of the samples being detected. The inlet and outlet-flow counting method overly relies on the accuracy of the detection device. Therefore, the pressure drop method was



adopted to measure the carbon sequestration effect of  $\mathrm{CO}_2\text{-CBM}$  in this study. The principle of the pressure drop method is that during the wet mineralization reaction process, the pressure drop inside the reactor is mainly caused by the dissolution of  $\mathrm{CO}_2$  and the mineralization reaction. Therefore, according to Equation 1, the pressure drop inside the reactor caused by the mineralization reaction can be calculated as follows (Wang et al., 2017; Montes-Hernandez et al., 2009).

$$P_{carbonatton} = P_{global} - P_{blank} \tag{1}$$

where  $P_{\rm carbonatton}$  represents the mineralization pressure drop, Pa;  $P_{\rm global}$  represents the total pressure drop, Pa;  $P_{\rm blank}$  represents the pressure drop of the blank solution, Pa. The amount of CO<sub>2</sub> absorbed by the mineralization reaction  $\rm m_{\rm CO2}$  (g-CO<sub>2</sub>/kg- CBM) can be calculated by Equation 2:

$$m_{\rm CO_2} = \frac{44 \cdot P_{\rm carbonatton} V_s}{ZRTm_{\rm CBM}} \tag{2}$$

where  $V_s$  represents the difference between the volume of the reaction vessel and the volume of the slurry, m³; Z is the compression factor of  $\mathrm{CO}_2$  gas, and Z=1 for an ideal gas at any temperature and pressure; R is the gas constant, with a value of 8.314 J/(mol·K); T is the reaction temperature, K;  $\mathrm{m}_{\mathrm{CBM}}$  is the mass of the slurry, kg.

### 2.3.2 Rheological properties

The rheological properties of CO<sub>2</sub>-CBM were tested using a rheometer (Anton paar MCR72, Graz, Austria), and the selected rotor model was ST22-4V-40. Figure 4 shows the working principle and specific parameters of the rheometer rotor, among which  $D=75~\rm mm,~d=22~\rm mm,~l_1=10~\rm mm,~l_2=40~\rm mm,~and~l_3=70~\rm mm.$  The rotor must be positioned at the center of the container's cross-sectional area, and its rotational speed gradually increased from 0 to  $150~\rm s^{-1}$  over a period of  $120~\rm s.$  Through multiple experiments, the evolution laws of rheological properties of CO<sub>2</sub>-CBM with different mass concentrations after standing for 10 min, 30 min, 1 h and 2 h were determined. The test results were fitted by using the rheological constitutive equation. Finally, the rheological properties of the freshly mixed backfill slurry were analyzed through yield stress and plastic viscosity.

### 2.3.3 Uniaxial compressive strength (UCS)

Specimens were prepared in accordance with the Chinese standard (GB/T17671-2021) (Guo et al., 2022). The  $CO_2$ -CBM slurry was poured into the standard cylindrical mold and placed on the vibrating table to remove any trapped air bubbles and ensure a smooth surface. The mold specification was  $\Phi$  50 mm × 100 mm. The samples were sealed with plastic wrap to avoid water evaporation from the mixture, and subsequently placed in a controlled environment chamber maintained at a constant temperature (20 °C) and humidity for curing periods of 3, 7, 14, and 28 days, respectively. After the curing time was reached, the UCS of the specimens was tested in accordance with the national standard GB/T1761-1999 using the TKA-WXY-10F fully automatic unconfined pressure gauge (Figure 4B). The cured sample was subjected to displacement loading at a constant speed of 0.5 mm/min. All tests were repeated three times, and the average UCS value was taken as the final value for further analysis.

### 2.3.4 Microscopic characteristics

To illustrate the evolution law of  $\rm CO_2\text{-}CBM$  with different mass concentrations, a large number of microscopic experiments were conducted to reveal the influence mechanism of mass concentration on the hydration reaction and the microstructure of  $\rm CO_2\text{-}CBM$ , including scanning electron microscopy (SEM) experiments, thermogravimetric analysis (TG/DTG), and mercury intrusion experiments (MIP). All microscopic samples were dried in a drying oven at 60 °C for 2 days after the designed curing time to remove free water until the quality was stable. Free water was removed from the sample to cease the cement hydration process. Furthermore, drying at this temperature did not result in cracking of the sample.

SEM: SEM can be used to qualitatively analyze the gel yield and microscopic morphology of samples. The samples were adhered to the conductive adhesive, and then gold spraying was used to improve the conductivity of the samples. The microscopic characteristics of samples with different mass concentrations at different curing times were observed using Sigma 360 produced by ZEISS in Germany. The fundamental principle of TG analysis relies on monitoring a material's mass change as temperature increases. In this technique,

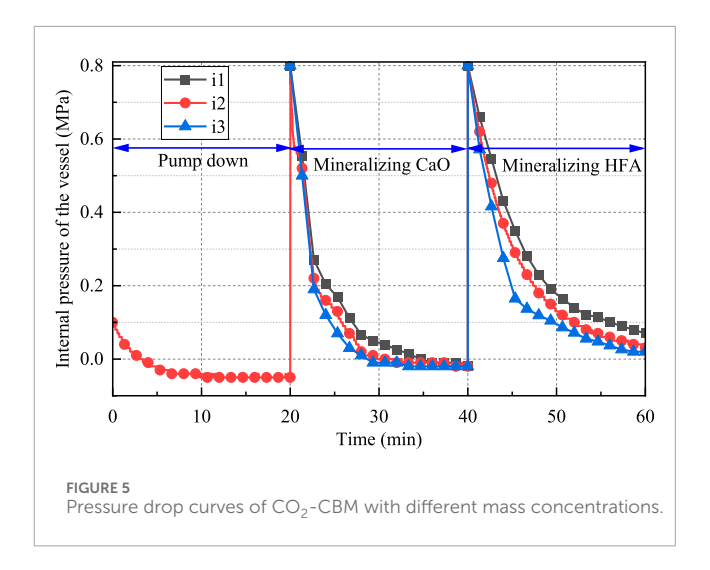
a decrease in mass within specific temperature ranges indicates the decomposition or volatilization of particular components. The samples were heated and analyzed using the STA 449 F5 thermogravimetric analyzer produced by Netzsch of Germany. Mercury Intrusion Porosimetry (MIP) was used to measure the intrusion volume of mercury under different pressures. The key parameters of the pore structure such as pore size distribution and total pore volume of the material were calculated, and MIP tests were conducted using AutoPore V 9620 produced by Micromeritics in the United States.

### 3 Results and discussion

# 3.1 Influence of mass concentration on the carbon sequestration performance of $CO_2$ -CBM

Figure 5 shows the pressure drop curves of CO<sub>2</sub>-CBM with different mass concentrations. The curves can be divided into three sections: the vacuuming stage (0-20 min), the CaO mineralization stage (20-40 min), and the HFA mineralization stage (40-60 min). During the vacuuming stage, the pressure within the reaction vessel is reduced to -0.5 MPa. During the CaO mineralization stage, the pressure in the reactor rapidly drops from 0.8 to -0.2 MPa. Moreover, as the mass concentration decreases, the pressure drop becomes even more rapid. However, the final pressure drop in each group is the same. This is because the CaO mineralization exhibits three stages. Firstly, CaO reacts with water to form Ca(OH)2, then CO<sub>2</sub> dissolution occurs, and finally CO<sub>2</sub><sup>2-</sup> reacts with Ca<sup>2+</sup> to form CaCO<sub>3</sub>. As the mass concentration decreases, a greater amount of water within the reactor is able to dissolve increased quantities of CO<sub>2</sub>, thereby increasing the collision probability of CO<sub>2</sub><sup>2</sup> with Ca<sup>2+</sup> and accelerating the formation of CaCO<sub>3</sub>. Therefore, the internal pressure of CO<sub>2</sub>-CBM with a low mass concentration drops more rapidly in the reactor. This finding is consistent with the previous conclusion on coal gangue (Zhang et al., 2025). Since each group reached the reaction equilibrium point in advance and the CaO content is the same, the total CaO mineralization amount of each group is the same. Through the calculation of Equations 1 and 2, the mineralization amount of CaO in each group at this stage is 540.3 g/kg, that is, the carbon sequestration amount of CO<sub>2</sub>-CBM is 48.6 g/kg.

During the HFA mineralization stage, the mineralization reaction rate also increases with the decrease of mass concentration, but there are differences in the final HFA mineralization amounts in different groups. This is because Ca<sup>2+</sup> in HFA is fixed in inert minerals, and its leaching requires a certain amount of time. At 60 min, the reaction equilibrium point has not been reached. The carbon sequestration amounts of HFA in groups i1, i2 and i3 are 109.8 g/kg, 131.8 g/kg and 153.8 g/kg, respectively. In other words, the carbon sequestration amounts of CO<sub>2</sub>-CBM with mass concentrations of 73%, 69% and 65% are 24.1 g/kg, 28.9 g/kg and 33.8 g/kg, respectively. Based on the two-stage mineralization, the carbon sequestration amounts of CO<sub>2</sub>-CBM with mass concentrations of 73%, 69%, and 65% are 72.7 g/kg, 77.5 g/kg, and 82.4 g/kg, respectively.



### 3.2 Rheological properties of CO<sub>2</sub>-CBMs

## 3.2.1 Rheological property evolution law of $CO_2$ -CBMs

As shown in Figure 6a, with the increase of shear rate, the rheological curves of CO2-CBM at different standing times exhibit similar evolution trends. These curves can be mainly divided into two stages: Stage I (0-30 seconds-1) and Stage II (30-150 s-1). In Stage I, the shear stress first increases and then decreases. This area is called the stress overshoot area, and the peak is called the ultimate yield stress ( $\tau_{max}$ ) (Jiang et al., 2019; Panchal et al., 2018). Moreover, this area becomes more obvious with the increase in the standing time. There are three reasons for stress overshoot. Firstly, the C-S-H produced by the hydration reaction hinders the cementation of particles. Secondly, the formation of crystals such as CaCO3 and AFT fills the gaps between particles, increasing the friction force. Finally, the seepage of free water reduces the lubricity between particles. In the initial stage, shearing the slurry necessitates the breakdown of both the C-S-H floc structure and the interlocking structure between particles. This process of structural disruption causes the shear stress to initially rise and then subsequently decline. The extended standing time leads to an increase in the formation of C-S-H flocs and crystals, as well as a greater amount of free water being released. Consequently, the stress overshoot phenomenon is more pronounced after standing for 2 h compared to a standing time of 10 min. After a standing time of 10 min,  $\tau_{max}$  is 207.72 Pa, while after a standing time of 2 h,  $\tau_{max}$  is 555.97 Pa, increasing by 2.68 times. This phenomenon proves that the slurry needs to overcome higher flow resistance from stationary state to a flowing one. In practical engineering applications, once the slurry stops flowing, a higher pumping power is required.

In Stage II, the shear force overcomes the initial flow resistance, and the slurry gradually becomes uniform, showing a linear growth trend in Stage II. The rheological parameters in this area can be analyzed using the Bingham model [Equation 3] (Gutierrez-Gonzalez et al., 2013).

$$\tau = \tau_0 + \mu \dot{\gamma} \tag{3}$$

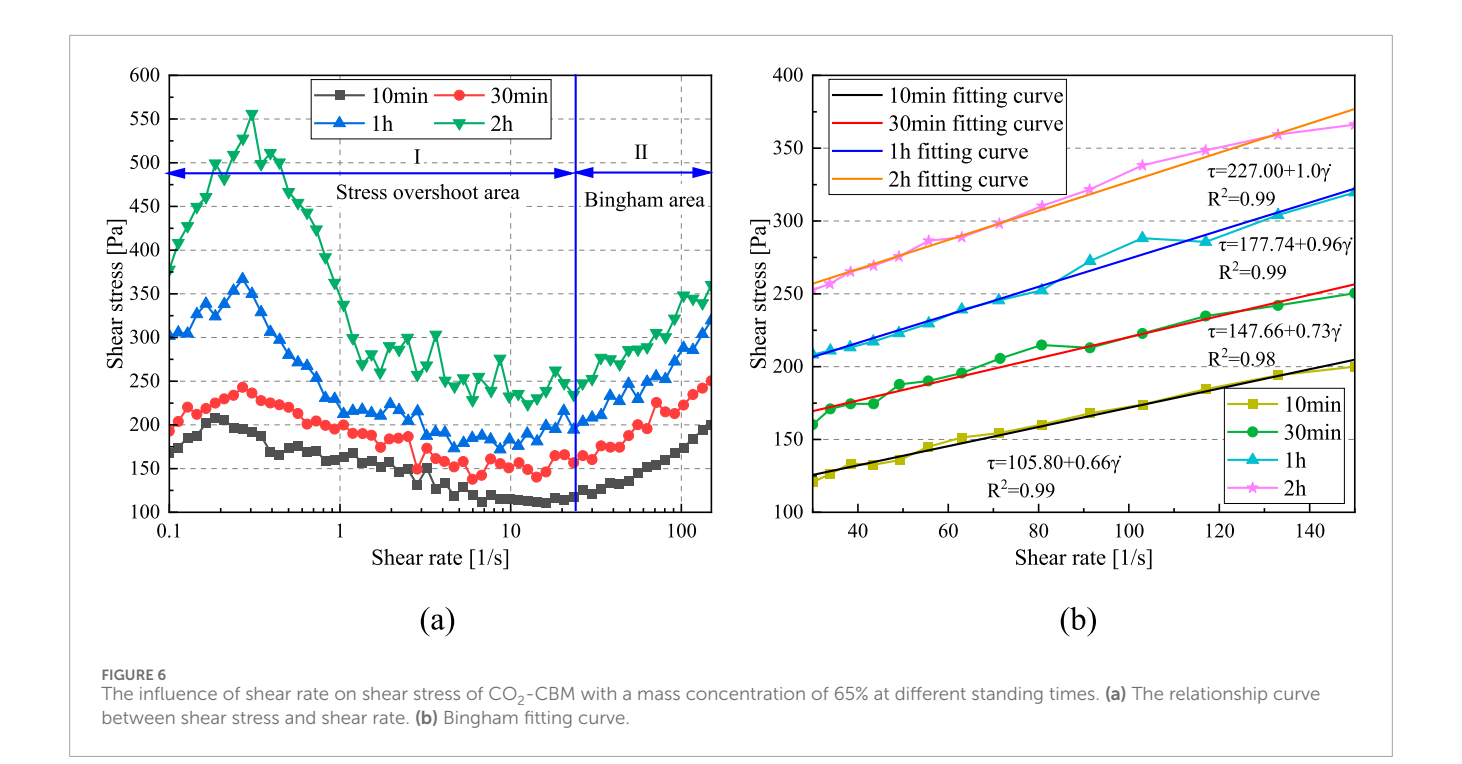


TABLE 3 Bingham parameters of  ${\rm CO_2}\text{-CBM}$  with a mass concentration of 65% at different standing times.

Standing time	Regression equation of the bingham model	τ <sub>0</sub> /Pa	η/Pa·s	R <sup>2</sup>
10 min	$\tau = 105.80 + 0.66 * \dot{\gamma}$	105.80	0.66	0.99
30 min	$\tau = 147.66 + 0.73 * \dot{\gamma}$	147.66	0.73	0.98
1 h	$\tau = 177.74 + 0.96 * \dot{\gamma}$	177.74	0.96	0.99
2 h	$\tau = 227.00 + 1.0 * \dot{\gamma}$	227.00	1.0	0.99

where  $\tau$  represents the shear stress, Pa;  $\tau_0$  is the yield shear stress, Pa;  $\mu$  represents plastic viscosity, Pa·s;  $\dot{\gamma}$  is the shear rate, s<sup>-1</sup>.  $\tau_0$  represents the minimum shear stress required for the fluid to start flowing, and  $\mu$  reflects the capacity of the fluid to resist deformation in a flowing state.

Table 3 and Figure 6b present the Bingham rheological parameters of  $CO_2$ -CBM with a mass concentration of 65% at different standing times. The regression coefficients  $R^2$  are all greater than 0.98, indicating that the model has a good fitting effect on the data. The yield stress and plastic viscosity of the slurry after a standing time of 10 min are 105.80 Pa and 0.66 Pa·s, respectively, while those after 2 h increase to 227.00 Pa and 1.0 Pa·s, respectively. It indicates that with the extension of the standing time, the yield stress and plastic viscosity of the slurry also increase significantly. The mechanism is also attributed to the progress of the hydration reaction and the precipitation of free water, which leads to an increase in the frictional force between particles.

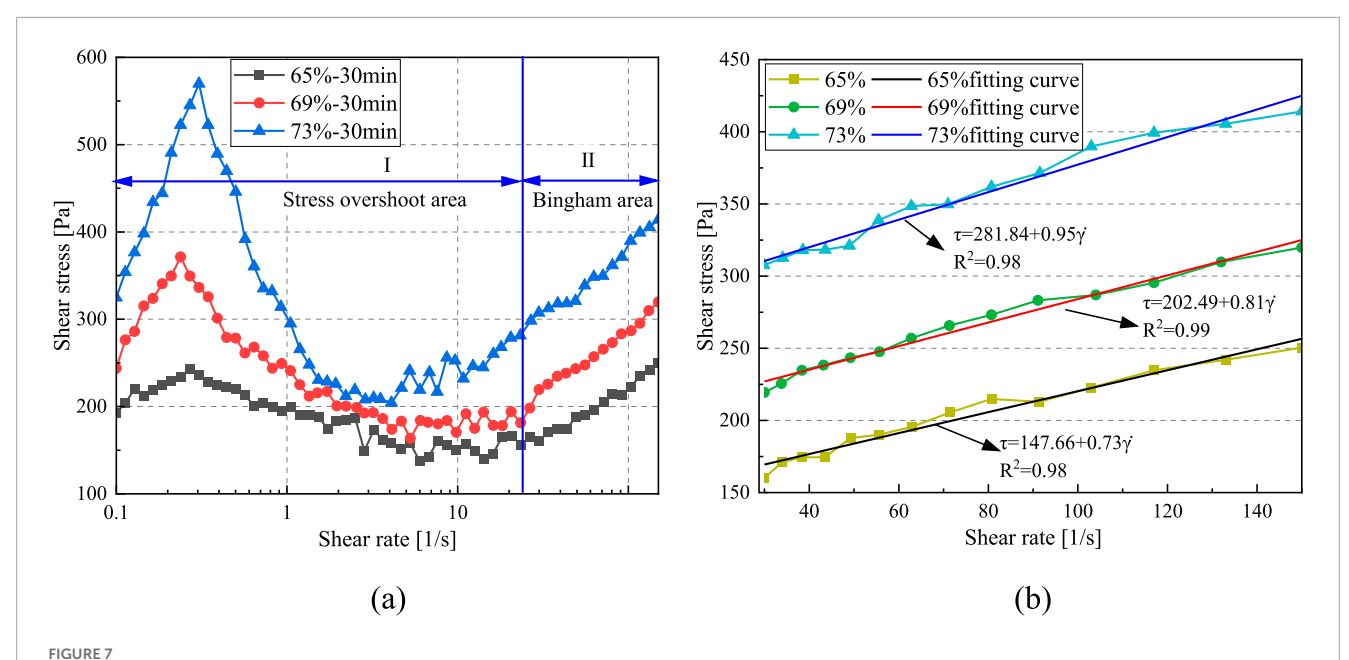
# 3.2.2 Influence of mass concentration on the rheological properties of CO<sub>2</sub>-CBM

As shown in Figure 7a, with the increase in shear rate, the rheological curves of  $CO_2$ -CBM with different mass concentrations after a standing time of 30 min. can also be divided into the stress overshoot area and the Bingham area. In the stress overshoot area, with the increase in mass concentration, the ultimate yield stress is greater. The ultimate yield stress  $\tau_{\rm max}$  of  $CO_2$ -CBM with a mass concentration of 65% after a standing time of 30 min is 242.98 Pa, while that of  $CO_2$ -CBM with a mass concentration of 73% increases to 569.8 Pa. A higher solid content reduces the amount of free water available to lubricate particles, thereby requiring a higher shear force to overcome the increased interlocking between them.

Table 4 and Figure 7b present the fitting results of the rheological curves of the slurry in Stage II based on the Bingham model. The fitting regression coefficients  $R^2$  are all greater than 0.98, indicating a good fitting effect. After a standing time of 30 min, the yield stress and plastic viscosity of CO<sub>2</sub>-CBM with a mass concentration of 65% are 147.66 Pa and 0.73 Pa·s, respectively; Those of CO<sub>2</sub>-CBM with a mass concentration of 69% and 73% increase to 202.49 Pa, 281.84 Pa, 0.81 Pa·s and 0.95 Pa·s, respectively. It indicates that the mass concentration has an extremely obvious influence on the rheological properties of the slurry.

# 3.3 Influence of mass concentration on the UCS of CO<sub>2</sub>-CBMs

Figure 8 shows the evolution law of UCS of  $\rm CO_2\text{-}CBMs$  with curing time. The results show that the UCS of the  $\rm CO_2\text{-}CBM$  increases with the increase in curing time. For example, the UCS of  $\rm CO_2\text{-}CBM$  with a mass concentration of 65%, 69%, and 73% after curing time of 7 days are 0.24 MPa, 0.31 MPa, and 0.40 MPa,



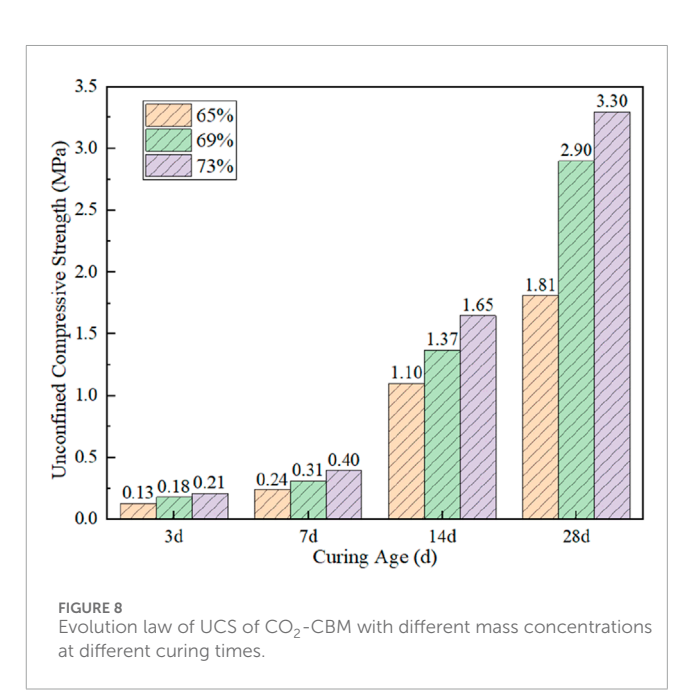
The influence of shear rate on shear stress of CO<sub>2</sub>-CBM at different mass concentrations after a standing time of 30 min. (a) The relationship curve between shear stress and shear rate. (b) Bingham fitting curve.

TABLE 4 Bingham parameters of  $CO_2$ -CBM at different mass concentrations after a standing time of 30 min.

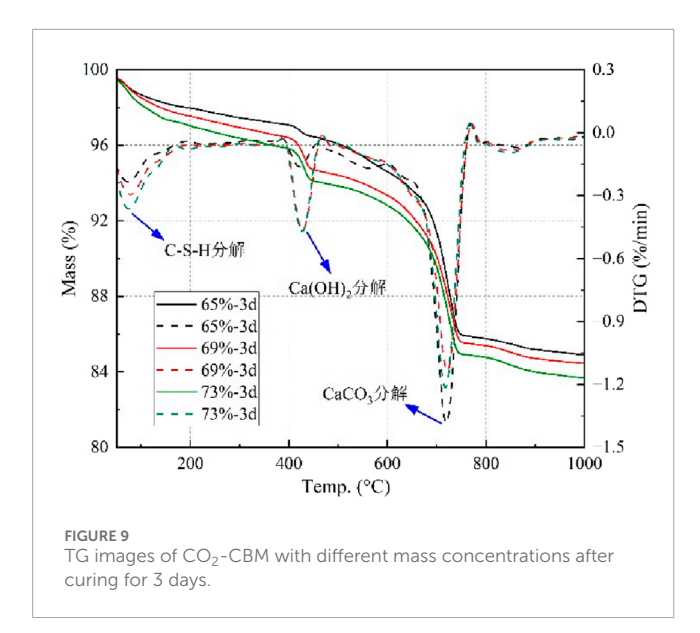
	3			
Mass concentration	Regression equation of the bingham model	τ <sub>0</sub> /Pa	η/Pa·s	R <sup>2</sup>
65%	$\tau = 147.66 + 0.73 * \dot{\gamma}$	147.66	0.73	0.98
69%	$\tau = 202.49 + 0.81 * \dot{\gamma}$	202.49	0.81	0.99
73%	$\tau = 281.84 + 0.95 * \dot{\gamma}$	281.84	0.95	0.98

respectively; After curing time of 28 days, those increase to 1.81 MPa, 2.90 MPa and 3.30 MPa, respectively. For conventional backfill materials, a 28-day UCS of 0.7–2.0 MPa is typically deemed sufficient. (Fall and Benzaazoua, 2005). Consequently, the CO<sub>2</sub>-CBM also demonstrates favorable mechanical properties. This is because, as the hydration reaction proceeds, the C-S-H gel gradually densifies, providing a higher bonding force between the particles (Yu et al., 2024; Zhan et al., 2014). Moreover, substances such as AFT, Ca(OH)<sub>2</sub>, and CaCO<sub>3</sub> produced by hydration fill the gaps between particles and play a supporting role in the material, thereby enhancing its strength (Hou et al., 2024).

With the increase in the mass concentration of  $\rm CO_2\text{-}CBM$ , the UCS of the backfill body at all ages shows an upward trend. When the curing time is 3 days, the UCS of  $\rm CO_2\text{-}CBM$  are 0.13 MPa, 0.18 MPa and 0.21 MPa respectively. This can be explained as follows: In a system with high concentration quality, the available free space is minimal; The C-S-H gel becomes densely packed within the gaps between aggregate particles, creating a more continuous and compact structure; Consequently, this leads to an increased amount



of C-S-H per unit mass of CO<sub>2</sub>-CBM. This finding can be confirmed by the TG analysis of CO<sub>2</sub>-CBM with different mass concentrations after curing time of 3 days. As shown in Figure 9, the TG curves of CO<sub>2</sub>-CBM at different mass concentrations gradually decrease with the increase in temperature, and the DTG curves show three peak values of weight loss rates respectively, located at 50 °C–150 °C, 350 °C–500 °C and 600 °C–780 °C. The three correspond to the pyrolysis of C-S-H gel, Ca(OH)<sub>2</sub> and CaCO<sub>3</sub>. It can be seen that with the increase in the mass concentration of CO<sub>2</sub>-CBM, the pyrolysis rate of C-S-H is faster, proving that there is more C-S-H in the unit



mass of  $\rm CO_2$ -CBM. At the third peak, the weight loss rate of  $\rm CO_2$ -CBM with a mass concentration of 65% is the fastest, followed by  $\rm CO_2$ -CBM with a mass concentration of 73%. This indicates that the highest content of  $\rm CaCO_3$  is  $\rm CO_2$ -CBM at a mass concentration of 65%, followed by that at a mass concentration of 73%, and the lowest is at 69%. This is because at a low mass concentration,  $\rm CO_2$ -CBM can consolidate more  $\rm CO_2$  in the carbon sequestration reaction, but its total carbon sequestration is relatively low.

In addition, the excess moisture in CO2-CBM with a low mass concentration leads to more interconnected pores between particles, while the hydration products in CO2-CBM with a high mass concentration fill fewer pores, resulting in a denser structure and a higher UCS. This phenomenon can be confirmed by Figure 10. For the specimens cured for 28 days, the specimens with a mass concentration of 65% have a distinct real-time flow peak, which reaches 0.022 mL/g at a pore diameter of 95.4 nm. However, the specimens with a mass concentration of 73% do not show a distinct peak. When the pore diameter is less than 349.3 nm, the realtime pore flow rate of the specimens with a mass concentration of 65% is all greater than that of the specimens with a mass concentration of 73%. Furthermore, when the pore size is less than 281.1 nm, the cumulative pore size flow rate of specimens with a mass concentration of 65% is significantly greater than that of specimens with a mass concentration of 73%. This indicates that the CO<sub>2</sub>-CBM with a low mass concentration has a higher porosity after 28 days of curing, resulting in its UCS being lower than that of specimens with a high mass concentration.

From the perspective of the micrometer scale, Figure 11 shows the differences in microstructure of  $\rm CO_2\text{-}CBM$  with different mass concentrations after curing for 28 days. It indicates that the slurry mass concentration has a significant impact on its microstructure. It can be seen that the particle surfaces of  $\rm CO_2\text{-}CBM$  with various mass concentrations are all covered with relatively dense C-S-H. However, in the sample with a mass concentration of 65%, the pore distribution is large and numerous, and hydration products such as ettringite (AFT) are difficult to fill them (Figure 11a), resulting in the gel being difficult to bond the particles. As the mass concentration increases, the pores gradually decrease

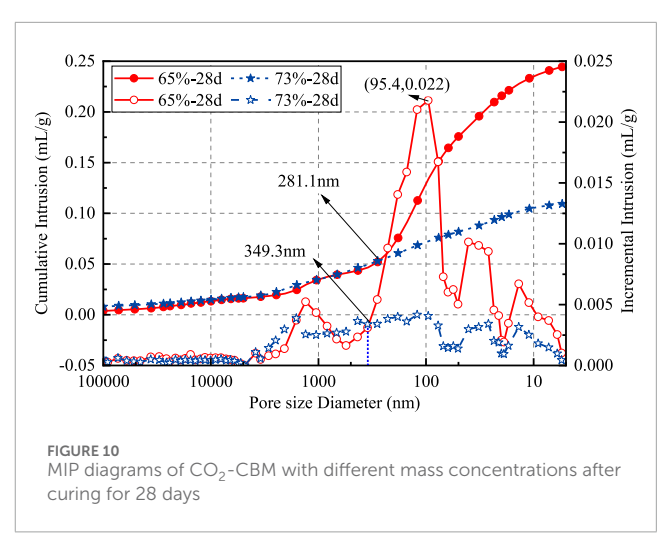
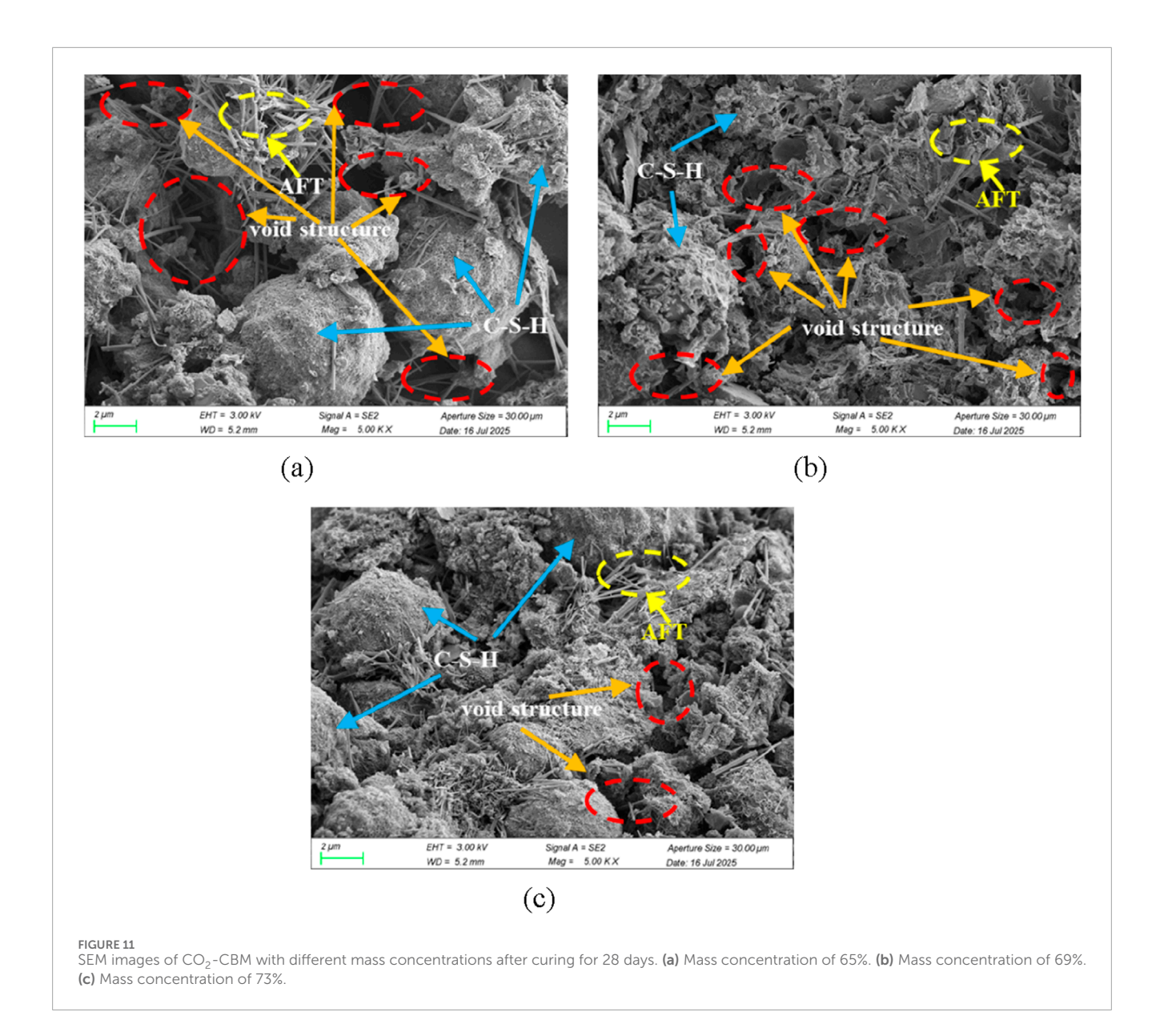


(Figure 11b) and are completely filled by hydration products such as AFT (Figure 11c), this allows the gel to bond the particles together, resulting in higher UCS.

### 4 Conclusion

This paper studies the carbon sequestration capacity, rheological properties and UCS of CO<sub>2</sub>-CBM with different mass concentrations, and reveals the intensity evolution mechanism through a series of microscopic experiments, drawing the following conclusions.

- Due to the high free water content in low-concentration slurry, the CO<sub>2</sub> dissolution efficiency is enhanced and the mineralization reaction rate is faster. Within a fixed period of time, the low-concentration slurry has a higher carbon sequestration capacity. The carbon sequestration capacity of 65% concentration CO<sub>2</sub>-CBM reaches 82.4 g/kg.
- 2. The shearing of the slurry after standing still requires the destruction of the C-S-H floc structure and the interlocking structure between particles, so the rheological curve shows a stress overshoot area. After standing for 2 h, the ultimate yield stress of the 65% concentration slurry was 555.97 Pa, the yield stress increased to 227 Pa, and the plastic viscosity increased to 1.0 Pa·s. The main reason is that the formation of hydration products and the precipitation of free water increase the friction between particles, so the ultimate yield stress, yield stress and plastic viscosity of the slurry increase. Therefore, it is necessary to avoid the pump being shut down for too long to prevent difficulty in restarting.
- 3. Under the same standing time, when the slurry mass concentration increased from 65% to 73%, the yield stress increased from 147.7 Pa to 281.8 Pa, and the plastic viscosity increased from 0.73 Pa·s to 0.95 Pa·s. Due to the high proportion of solid phase and weakened free water lubrication effect, the flow resistance of high-concentration slurry increases significantly.
- 4. Due to the ongoing hydration reaction, the UCS of samples of all concentrations increased with the curing time. The



strength of the 73% concentration sample was only 0.21 MPa at 3 days and reached 3.30 MPa at 28 days. As the concentration increases, the strength of the sample also rises. This is because the high-quality concentration slurry has a higher C-S-H gel content, lower porosity and a dense structure. However, the presence of a large number of interconnected pores in a low-concentration slurry weakens the cementation strength.

### Data availability statement

The raw data supporting the conclusions of this article will be made available by the authors, without undue reservation.

### **Author contributions**

FJ: Investigation, Writing – original draft. XW: Investigation, Methodology, Writing – original draft. ZL: Data curation, Validation, Writing – review and editing. HP: Software, Writing – review and editing. TS: Funding acquisition, Visualization, Writing – review and editing.

### **Funding**

The author(s) declare that no financial support was received for the research and/or publication of this article.

### Conflict of interest

Author FJ was employed by China National Coal Group Corporation.

Authors XW, HP, and TS were employed by China Coal Energy Research Institute Co., Ltd.

The remaining author declares that the research was conducted in the absence of any commercial or financial relationships that could be construed as a potential conflict of interest.

### Generative Al statement

The author(s) declare that no Generative AI was used in the creation of this manuscript.

### References

Chen, Q., Zhu, L., Wang, Y., Chen, J., and Qi, C. (2022). The carbon uptake and mechanical property of cemented paste backfill carbonation curing for low concentration of CO2. *Sci. Total Environ.* 852, 158516. doi:10.1016/j.scitotenv.2022.158516

Fall, M., and Benzaazoua, M. (2005). Modeling the effect of sulphate on strength development of paste backfill and binder mixture optimization. *Cem. Concr. Res.* 35, 301–314. doi:10.1016/j.cemconres.2004.05.020

Gao, Y. J., Huang, H. J., Tang, W. J., Liu, X. Y., Yang, X. Y., and Zhang, J. B. (2015). Preparation and characterization of a novel porous silicate material from coal gangue. *Microporous Mesoporous Mater.* 217, 210–218. doi:10.1016/j.micromeso.2015.06.033

Guo, L., Zhou, M., Wang, X., Li, C., and Jia, H. (2022). Preparation of coal gangue-slag-fly ash geopolymer grouting materials. *Constr. Build. Mater.* 328. doi:10.1016/j.conbuildmat.2022.126997

Guo, Y., Zhang, J., Long, K., Ma, J., Gao, Y., and Li, B. (2024). Experimental study on CO2 sequestration capacity and mechanical characteristics evolution of solid wastes based carbon-negative backfill materials. *Constr. Build. Mater.* 440, 137457. doi:10.1016/j.conbuildmat.2024.137457

Gutierrez-Gonzalez, S., Alonso, M. M., Gadea, J., Rodriguez, A., and Calderon, V. (2013). Rheological behaviour of gypsum plaster pastes with polyamide powder wastes. *Constr. Build. Mater.* 38, 407–412. doi:10.1016/j.conbuildmat.2012.08.034

Heping, X., Jixiong, Z., Feng, G., Baoyi, L., Cunbao, L., Yachen, X., et al. (2024). Theory and technical conception of carbon-negative and high-efficient backfillmining in coal mines. *J. China Coal Soc.* 49, 36–46. doi:10.13225/j.cnki.jccs.2023.1091

Heping, X., Mingzhong, G., Jianzhong, L., Hongwei, Z., Ruixin, Z., Peipei, C., et al. (2018). Research on exploitation and volume estimation of underground space in coal mines. *J. China Coal Soc.* 43, 1487–1503. doi:10.13225/j.cnki.jccs.2018.0547

Hou, Y., Kong, P., Yang, K., Yin, S., Yu, X., Wang, Y., et al. (2024). Enhancing performance and structural integrity of cemented paste backfill: rheological behavior, strength characteristics, and microstructural dynamics. *CASE Stud. Constr. Mater.* 20. doi:10.1016/j.cscm.2024.e03367

Huang, M., Cai, S., Chen, L., and Tang, S. (2022). Multi-response robust parameter optimization of cemented backfill proportion with ultra-fine tailings. *MATERIALS* 15, 6902. doi:10.3390/ma15196902

Huo, B., Zhang, J., Li, M., Zhou, N., Qiu, X., Fang, K., et al. (2023). Effect of CO2 mineralization on the composition of alkali-activated backfill material with different coal-based solid wastes. *Sustainability* 15. doi:10.3390/su15064933

Huo, B., Zhang, Q., Li, M., and Xing, S. (2024). Using recycled gangue to capture CO2 and prepare alkali-activated backfill paste: adsorption and microevolution mechanisms. *FUEL* 358. doi:10.1016/j.fuel.2023.130194

Jiang, G., Wu, A., Wang, Y., and Li, J. (2019). The rheological behavior of paste prepared from hemihydrate phosphogypsum and tailing. *Constr. Build. Mater.* 229. doi:10.1016/j.conbuildmat.2019.116870

Lang, L., Shuangming, W., Mengbo, Z., Bo, Z., Dongzhuang, H., Chao, H., et al. (2022). CO2 storage-cavern construction and storage method based on functional backfill. *J. China Coal Soc.* 47, 1072–1086. doi:10.13225/j.cnki.jccs.xr21.1558

Minggao, Q., Jialin, X., and Jiachen, W. (2018). Further on the sustainable mining of coal. *J. China Coal Soc.* 43, 1–13. doi:10.13225/j.cnki.jccs.2017.4400

Montes-Hernandez, G., Perez-Lopez, R., Renard, F., Nieto, J. M., and Charlet, L. (2009). Mineral sequestration of CO2 by aqueous carbonation of coal combustion fly-ash. *J. Hazard. Mater.* 161, 1347–1354. doi:10.1016/j.jhazmat.2008.04.104

Any alternative text (alt text) provided alongside figures in this article has been generated by Frontiers with the support of artificial intelligence and reasonable efforts have been made to ensure accuracy, including review by the authors wherever possible. If you identify any issues, please contact us.

### Publisher's note

All claims expressed in this article are solely those of the authors and do not necessarily represent those of their affiliated organizations, or those of the publisher, the editors and the reviewers. Any product that may be evaluated in this article, or claim that may be made by its manufacturer, is not guaranteed or endorsed by the publisher.

Panchal, S., Deb, D., and Sreenivas, T. (2018). Variability in rheology of cemented paste backfill with hydration age, binder and superplasticizer dosages. *Adv. POWDER Technol.* 29, 2211–2220. doi:10.1016/j.apt.2018.06.005

Qi, C., and Fourie, A. (2019). Cemented paste backfill for mineral tailings management: review and future perspectives. *Miner. Eng.* 144. doi:10.1016/j.mineng.2019.106025

Ren, S., Jiao, X., Zheng, D., Zhang, Y., Xie, H., and Zhang, R. (2025). Impact of carbon neutrality goals on China's coal industry: mechanisms and evidence. *ENERGIES* 18. doi:10.3390/en18071672

Shuangming, W., Yanjun, S., Shijie, S., Lang, L., Linjun, G., and Jiangbo, W. (2023). Change of coal energy status and green and low-carbon development under the "dual carbon" goal. *J. China Coal Soc.* 48, 2599–2612. doi:10.13225/j.cnki.jccs.cn23.0260

Shuangming, W., Lang, L., Mengbo, Z., Yanjun, S., Qingmin, S., Qiang, S., et al. (2024). New way for green and low-carbon development of coal industry under thetarget of "daul-carbon". *J. China Coal Soc.* 49, 152–171. doi:10.13225/j.cnki.jccs.YH23.1690

Tingye, Q., Siyuan, C., Guorui, F., Linfei, W., Hongtao, X., Lubin, L., et al. (2025). Preparation of alkali-activated steel slag-fly ash based full solid waste filling material and strength formation mechanism research. *Coal Sci. Technol.* 53, 236–249. doi:10.12438/cst.2025-0316

Wang, T., Huang, H., Hu, X., Fang, M., Luo, Z., and Guo, R. (2017). Accelerated mineral carbonation curing of cement paste for CO2 sequestration and enhanced properties of blended calcium silicate. *Chem. Eng. J.* 323, 320–329. doi:10.1016/j.cej.2017.03.157

Wang, M., He, X., and Yang, K. (2023). Mechanical properties and damage characteristics of coal-based solid waste paste filling materials with different moisture content. *Sustainability* 15. doi:10.3390/su15021523

Wang, B., Cheng, H. G., Liu, X., Di, Z. C., Song, H. P., Zhang, D. K., et al. (2025). CO2 mineralized full solid waste cementitious material for coal mine goaf filling and carbon sequestration potential assessment. *Engineering* 48, 70–80. doi:10.1016/j.eng.2025.02.017

Wei, Z., Yang, K., He, X., Zhang, J. Q., and Hu, G. C. (2022). Experimental study on the optimization of coal-based solid waste filling slurry ratio based on the response surface method. *Materials* 15, 5318. doi:10.3390/ma15155318

Weiji, S., Lang, L., Zhiyu, F., Mengbo, Z., Geng, X., Wei, H., et al. (2024). Technique of wet carbonation of modified magnesium slag chemical industry and engineering progress, 43, 2161–2173. doi:10.16085/j.issn.1000-6613.2023-0660

Xu, Y. J., and Ma, L. Q. (2024). Characteristics of overburden migration under continuous extraction and continuous backfill mining method with CO2 mineralized filling materials. *J. Clean. Prod.* 440. doi:10.1016/j.jclepro.2024.140920

Xu, Y., Ma, L., Wang, L., Ngo, I., and Wang, Y. (2025a). Continuous extraction and continuous backfill for gaseous and mineralized dual  $\rm CO_2$  sequestration and water-preserving coal mining. Geomechanics Geophys. Geo-Energy Geo-Resources 11. doi:10.1007/s40948-025-00957-z

Xu, Y., Ma, L., Wang, Y., Zhai, J., and Zhao, Z. (2025b). Strata migration and fracture development under continuous extraction and continuous backfill with  $\rm CO_2$  mineralized backfill materials. Geomechanics Geophys. Geo-Energy Geo-Resources 11. doi:10.1007/s40948-025-00970-2

Yu, K., Ma, L., Huo, B., Ngo, I., Wu, Y., and Zhai, J. (2024). Study on the fluidity and mechanical properties of multi-source coal-based solid waste (MCSW) filling material. J. Mater. Res. TECHNOLOGY-JMR&T 28, 2924–2934. doi:10.1016/j.jmrt.2023.12.225

Zhan, B., Poon, C. S., Liu, Q., Kou, S., and Shi, C. (2014). Experimental study on CO  $_2$  curing for enhancement of recycled aggregate properties. Constr. Build. Mater. 67, 3–7. doi:10.1016/j.conbuildmat.2013.09.008

Zhang, J., Yang, K., He, X., Wei, Z., Zhao, X., and Fang, J. (2022). Experimental study on strength development and engineering performance of coal-based solid waste paste filling material. METALS~12.~doi:10.3390/met12071155

Zhang, J., Li, B., Xie, Y., Li, C., Zhou, N., Guo, Y., et al. (2025). Carbon negative backfill mining in coal mines for carbon neutralization: Chemical carbon

fixation performances with mineralized gangue. Int. J. ROCK Mech. Min. Sci. 186. doi:10.1016/j.ijrmms.2024.106016

Zhu, L., Liu, C., Duan, G., Liu, Z., Shen, L., Zhou, Y., et al. (2025). Investigation on the activation mechanisms of coal gangue and the corresponding CO2 mineralization potential. *Front. Mater.* 12. doi:10.3389/fmats.2025.1567799

Zou, X., Zhang, Y., Liu, B., Xu, X., Lu, Z., and Jiang, W. (2023). Study on mechanical properties and ratio parameter optimization of fly ash wet shotcrete under the influence of multiple factors. *CASE Stud. Constr. Mater.* 19. doi:10.1016/j.cscm.2023.e02679